Journal of Materials Chemistry B

PAPER

View Article Online
View Journal | View Issue

Cite this: J. Mater. Chem. B, 2014, 2, 1344

The influence of fluorocarbon chain and phosphorylcholine on the improvement of hemocompatibility: a comparative study in polyurethanes†

Dongsheng Tan, Zhen Li, Xuelin Yao, Chunlan Xiang, Hong Tan* and Qiang Fu*

Received 19th October 2013
Accepted 2nd December 2013

DOI: 10.1039/c3tb21473g

www.rsc.org/MaterialsB

To study the influence of fluorinated surfaces and biomimetic surfaces on the improvement of the blood compatibility of polymers, three monomers containing a fluorinated tail and/or phosphorylcholine groups were designed and synthesized, and were then introduced into polyurethanes based on 4,4′-diphenylmethane diisocyanate (MDI), poly(tetramethylene glycol) (PTMG) and 1,4-butanediol (BDO) *via* end-capping. The bulk and surface characterization of the polyurethanes was carried out by dynamic mechanical analysis (DMA), Fourier transform infrared spectroscopy (FTIR), X-ray photoelectron spectroscopic analysis (XPS), atomic force microscope (AFM), and water contact angle measurements. The results indicate that the fluorocarbon chains can drive the phosphorylcholine groups to aggregate at the surface of polyurethane, and the two components show spontaneous arrangement to adapt to the environment when in contact with water. The preliminary evaluation of hemocompatibility was carried out *via* fibrinogen adsorption and platelet adhesion. The fluorocarbon chains and phosphorylcholine groups showed a synergistic effect on the improvement of hemocompatibility.

1. Introduction

Various polymers used in the biomaterials field need to be modified to improve their biocompatibility, mechanical properties, hydrolysis resistance properties, or other functionalities. In blood contacting materials, most research strategies consist of modulating the interface by modifying the synthetic graft surface properties, with the aim of improving their hemocompatibility.[1–6] For instance, polyurethanes (PU) are now widely used in biomedical apparatus and instruments because of their relatively good antithrombogenicity, excellent compliance, and beneficial physical/mechanical properties. However, the compatibility of PU with blood is not sufficient for making small-diameter vascular prostheses for *in vivo* applications,[3,7] and among the various modification methods, surface fluorination and surface biomimetic design are two efficient ways for improving its hemocompatibility.

It is well known that fluorocarbon chains exhibit unique characteristics, such as low surface energy, oxidative stability, and good water and oil repulsion.[4,8] As a result, a large number of fluorinated polymers have been found to be relatively hemocompatible. Xie *et al.* applied a fluorinated alcohol to end-cap poly(carbonate urethane)s, and the fluorinated poly(carbonate urethane)s revealed a unique bilayered surface structure which effectively improved the biostability and antiplatelet adhesion performance of this kind of polyurethane.[9] Fluorocarbon chains have also been introduced into the chain extender (in the hard segment) or the soft segment of polyurethanes.[10,11] The fluorocarbon chains could usually enhance the phase separation and migrate to the top surface, resulting in polyurethane samples exhibiting low surface energies and good blood compatibility. In fact, an *in vitro* platelet test has shown that the platelet compatibility of polyurethanes could be improved when the fluorocarbon oligomers were directly grafted onto the surface of polyurethanes.[12,13]

Introducing phospholipid analogues to form biomembrane mimicking polymers is another effective way to improve hemocompatibility by suppressing protein adsorption, platelet adhesion, and platelet activation on the surface of materials.[14–17] It is known that surface characteristics always play a decisive role in the blood compatibility of biomaterials, and the free and bound water on the surface of biomimetic polymers have been proven to play a crucial role in the outstanding biocompatibility.[18,19] Therefore, the phospholipid moieties should be designed to appear at the interface of polyurethane surfaces in order to function. For example, Iwasaki *et al.* prepared semi-interpenetrating polymer networks (IPNs) by the radical polymerization of diffused 2-methacryloyloxyethyl phosphorylcholine (MPC) in segmented polyurethane membranes;[20] Lee *et al.* used

College of Polymer Science and Engineering, State Key Laboratory of Polymer Materials Engineering, Sichuan University, Chengdu 610065, China. E-mail: qiangfu@scu.edu.cn; hongtan@scu.edu.cn; Fax: +86-28-85405402; Tel: +86-28-85460961

† Electronic supplementary information (ESI) available. See DOI: 10.1039/c3tb21473g

a poly(MPC-*co*-*n*-butyl methacrylate) solution to coat polyurethane surfaces to form a phospholipid interface, which showed a qualitative improvement in hemocompatibility during implantation.[5]

Both the fluorocarbon chain and phosphorylcholine have been demonstrated to effectively improve the blood compatibility of polymers by being introduced on their surfaces. It is unclear, however, which is more effective in the improvement of hemocompatibility, or if a synergistic effect can occur between them when they both appear in the same polymer surface? This motivated us to study the influence of fluorocarbon chains and phosphorylcholine on the improvement of blood compatibility in polyurethanes. In the present work, four kinds of polyurethanes with different chain ends (fluorocarbon chain and/or phosphorylcholine) were synthesized and characterized to explore the mechanism of the anticoagulation effect through comparison.

2. Experimental

2.1. Materials

2-Chloro-1,3,2-dioxaphospholane-2-oxide (COP, 95%) was purchased from Acros Organics. 2,2,3,3,4,4,5,5,6,6,7,7,8,8,8-Pentadecafluorooctanoicacid (95%), 5-amino-1-pentanol (95%), and dibutyltin dilaurate (DBTDL, 95%) were purchased from Aldrich. 4,4′-Diphenylmethane diisocyanate (MDI, Aladdin) and 1,4-butanediol (BDO, Aladdin) were used as received. Poly(tetramethylene glycol) (PTMG, M_w = 1000, obtained from Aldrich) was dehydrated at 100 °C for 4 h under vacuum. Other reagents and solvents were all obtained from Kelong Co. (Chengdu, China) in AR grade and were used as received.

2.2. Instrumentation

^{1}H NMR spectra were recorded on a Varian Unity INOVA (400 MHz) spectrometer, using tetramethylsilane (TMS) as an internal standard, and $CDCl_3$ or DMSO-d_6 as solvents. Mass spectra (MS) were obtained on a TSQ Quantum Ultra LC/MS/MS system (San Jose, CA, USA), and the electrospray ionization source was run in positive ion mode for all experiments. Gel permeation chromatography (GPC) was performed with a Waters-1515 apparatus using *N*,*N*-dimethylformamide (DMF)–LiBr as eluent. The molecular weights are relative to polymethyl methacrylate (PMMA) standards. The sample concentration was 2–3 mg mL^{-1}, and the flow rate was 1.000 mL min^{-1} at 40 °C. XPS was carried out on an XSAM-800 electron spectrometer equipped with a Mg Kα achromatic X-ray source (20 kV, 10 mA). The contents of phosphorus (P) and fluorine (F) were detected by an inductive coupled plasma emission spectrometer (ICP-AES, IRIS 1000, Thermo Fisher Scientific) and an ion chromatograph (ICS-90, DIONEX). Three samples were tested. The thermal transitions of the PUs were measured by dynamic mechanical analysis (Q800, TA Instruments-Waters LLC). Fourier transform infrared (FTIR) spectroscopy analysis was performed on a Nicolet-6700 spectrophotometer equipped with a Ge prism at an incident angle of 45°. AFM measurements were performed on an SPA400/SPI3800N (Seiko Instruments Inc.) with a tapping mode of 0.4–0.7 amplitude at room temperature. Contact angles of the samples were measured using the sessile drop method with a digital optical contact angle meter DSA100 (KRUSS GmbH, Germany) with 3 μL of water at 25 °C and relative humidity of 80%. Six films were tested for each sample.

2.3. Synthesis

2.3.1. Synthesis of *tert*-butyl 2-(2,2,3,3,4,4,5,5,6,6,7,7,8,8,8-pentadecafluorooctanamido) ethylcarbamate. A solution of 2,2,3,3,4,4,5,5,6,6,7,7,8,8,8-pentadecafluorooctanoicacid (**a**, 10 g, 24.2 mmol) and *N*-methylmorpholine (2.92 mL, 26.6 mmol) in anhydrous tetrahydrofuran (100 mL) was cooled to −15 °C, then isobutyl chlorocarbonate (3.17 mL, 5.0 mmol) was added. After the mixture was stirred for 10 min, *N*-boc-ethylenediamine (BDA) (**b**, 3.87 g, 24.2 mmol) in 10 mL anhydrous tetrahydrofuran was added dropwise to the reaction mixture. The reaction mixture was stirred for 2 h at room temperature and the solvent was removed using a rotary evaporator. Then the residue was dissolved in ethyl acetate. The solution was washed with dilute HCl, brine and distilled water, dried over $MgSO_4$, filtered under vacuum and evaporated in a vacuum to give crude **c**. The crude **c** was purified by silica gel column chromatography using a gradient of petroleum ether–ethyl acetate to yield 6.8 g of **c** (50.5%, R_f = 0.61 in 60% petroleum ether–ethyl acetate).

APCI MS (positive) *m*/*z*: theoretical 556 g mol^{-1}, observed 579 g mol^{-1}.

^{1}H NMR ($CDCl_3$, 400 MHz) δ ppm: 1.44 (s, 9H, –C(CH_3)$_3$), 3.36–3.41 (m, 2H, –CH_2–), 3.45–3.50 (m, 2H, –CH_2–), 4.92 (s, 1H, –NH–), 7.95 (s, 1H, –NH–).

2.3.2. Synthesis of *N*-(2-aminoethyl)-2,2,3,3,4,4,5,5,6,6,7,7,8,8,8-tetradecafluorooctanamide. Compound **c** (5.0 g, 9.0 mmol) was dissolved in 50 mL of ethyl acetate, 20 mL of saturated HCl–ethyl acetate was added, and the mixture was stirred at ambient temperature for 1 h. After evaporation of the solvent, ethyl ether (3 × 50 mL) was added to the residue and the precipitated white crude product was collected by filtration. Then, the crude product was dissolved in methanol, and adjusted to pH 10 by the addition of 1 N $NaHCO_3$. After the removal of the methanol under vacuum, the *N*-(2-aminoethyl)-2,2,3,3,4,4,5,5,6,6,7,7,8,8,8-tetradecafluorooctanamide (FA) was extracted with ethyl acetate and further washed with brine and distilled water, dehydrated over anhydrous $MgSO_4$, filtered under vacuum and evaporated in a vacuum to yield 3.5 g of FA (85.3%).

APCI MS (positive) *m*/*z*: theoretical 456 g mol^{-1}, observed 457 g mol^{-1}.

^{1}H NMR (DMSO, 400 MHz) δ ppm: 2.89 (t, 2H, –CH_2N–), 3.43 (t, 2H, –NCH_2–), 5.32 (t, 1H, –NH–), 7.85 (br, 2H, –NH_2).

2.3.3. Synthesis of *tert*-butyl-5-hydroxypentylcarbamate. To a solution of 5-amino-1-pentanol (**d**, 10.3 g, 0.1 mol) in dichloromethane (150 mL) was added dropwise a solution of di-*tert*-butyl dicarbonate (**e**, 21.8 g, 0.1 mol) in dichloromethane (50 mL) with stirring for 30 min, and then the mixture stirred for 24 h at room temperature. The volatile components were evaporated, and the residue was dissolved in ethyl acetate and further washed twice with 0.5 M citric acid and once with H_2O. After the mixture was dried ($MgSO_4$) and the solvent evaporated,

the residue was evaporated in a vacuum to yield an oil (**f**) (17.5 g, 86.2%).

APCI MS (positive) *m*/*z*: theoretical 204 g mol^{-1}, observed 205 g mol^{-1}.

^{1}H NMR ($CDCl_3$, 400 MHz) δ ppm: 1.25 (t, 2H, –CH_2OH), 1.44 (s, 9H, –C(CH_3)$_3$), 1.51 (m, 2H, –CH_2–), 1.59 (m, 2H, –CH_2–), 1.65 (s, 1H, –OH), 3.13 (q, 2H, –CH_2NH–), 3.65 (m, 2H, –CH_2–), 4.56 (s, 1H, –NH–).

2.3.4. Synthesis of 5-aminopentyl-2-(trimethylammonio) ethyl phosphate. Compound **f** (10.0 g, 49.0 mmol) and triethylamine (7.5 mL, 53.9 mmol) were dissolved in anhydrous tetrahydrofuran (80 mL). After cooling the solution down to −15 °C, COP (7.0 g, 49.0 mmol) dissolved in anhydrous tetrahydrofuran (10 mL) was added dropwise to the stirred solution under nitrogen. The temperature of the reaction mixture was maintained at −15 °C for 1 h and then allowed to slowly warm up to room temperature. The triethylammonium chloride precipitate was filtered off and washed with anhydrous tetrahydrofuran. The filtrate was evaporated under vacuum to give the residue as a colorless oil. The residue was dissolved in 60 mL dry acetonitrile and transferred to a 100 mL glass pressure bottle. After the pressure bottle was cooled to −18 °C, excess trimethylamine was rapidly added to the solution. The pressure bottle was then sealed and maintained at 60 °C for 24 h. Subsequently the solution was evaporated under vacuum to produce a viscous liquid, and then dissolved in methanol (20 mL) followed by the addition of saturated HCl–ethyl acetate (10 mL). The mixture was stirred for 2 h, concentrated under reduced pressure, washed with diethyl ether several times, dissolved in methanol (20 mL), adjusted to pH 9 by the addition of saturated sodium bicarbonate solution, and filtered. The filtrate was concentrated under reduced pressure and the crude product was purified by flash column chromatography (reverse phase silica gel, water : methanol = 10 : 1) to yield APPC as a white solid (10.2 g, 38.1 mmol, 78%).

APCI MS (positive) *m*/*z*: theoretical 268 g mol^{-1}, observed 269 g mol^{-1}.

^{1}H NMR (DMSO, 400 MHz) δ ppm: 1.38 (m, 2H, –CH_2–), 1.51 (m, 2H, –CH_2–), 1.60 (m, 2H, –CH_2–), 2.74 (t, 2H, –C$H_2$$NH_2$), 3.15 (s, 9H, –$N^+$($CH_3$)$_3$), 3.55 (t, 2H, –$CH_2N^+$), 3.68 (m, 2H, –$CH_2$O–), 4.05 (s, 2H, –O$CH_2$–), 8.20 (s, 2H, –$NH_2$).

^{13}C NMR (D_2O, 200 MHz) δ ppm: 19.5 (–CH_2–), 23.9 (–CH_2–), 26.7 (–CH_2–), 36.9 (–CH_2NH_2), 51.4 (–N^+(CH_3)$_3$), 56.8 (–CH_2N^+), 56.9 (–CH_2O–), 63.5 (–OCH_2–).

2.3.5. Synthesis of polyurethanes. The control polyurethane based on a 3 : 2 : 1 molar ratio of MDI : PTMG : BDO, and end-capped polyurethanes based on a 3 : 2 : 0.5 : 1 molar ratio of MDI : PTMG : BDO : end-capping reagent, were prepared by solution polymerization in a suitable solvent with DBTDL catalyst. All polyurethanes were synthesized by similar methods. A representative synthesis of PU-PC (PTMG-MDI-BDO-PC) is described as follows.

In the first reaction step, MDI and 0.5% DBDTL were added to the stirred toluene solution of PTMG under a dry nitrogen atmosphere at 60 °C. The reaction was maintained at 60 °C for 2 h. In the second step, the chain extender (BDO) was added to the reaction solution, while the temperature was kept at 70 °C for 1 h. Following this, APPC dissolved in DMF was added to the mixture and stirred at 80 °C for 1 h. The solution was then cooled to room temperature. The polymer was precipitated in a methanol–distilled water mixed solvent (v/v = 4 : 1) to remove any residual APPC and the low molecular weight fraction, then dried in an oven for 24 h, followed by drying at 60 °C under vacuum for 48 h.

The reaction scheme for the synthesis of the polyurethanes is shown in Scheme 2. The characteristics of the polymer (PU-PC) are summarized here:

FTIR (neat, cm^{-1}): 3297 (NH); 2940, 2856, 2799 (CH_2); 1728, 1706 (carbonyl of NHCOO); 1651 (carbonyl of NHCONH); 1221, 1103 (C–O–C).

^{1}H NMR (DMSO, 400 MHz) δ ppm: 1.24 (s, –CH_2–), 1.49 (m, –CH_2–), 3.13 (s, –N^+(CH_3)$_3$), 3.24 (br, –CH_2–), 3.34 (m, –CH_2OCH_2–), 3.78 (s, Ar-CH_2-Ar), 4.06 (t, –$COOCH_2$), 7.08, 7.34 (m, Ar-H), 9.50 (s, –NHC=O).

2.3.6. Sample preparation. Films used for testing were coated onto a clean glass disk from 10 wt% polymer solutions in DMF. The solvent was evaporated in an oven at 60 °C for 24 h, and the films were further dried in a vacuum oven at 60 °C for 48 h. The films were approximately 0.3 mm thick.

2.3.7. Protein adsorption assay. The adsorption of human fibrinogen onto the films was evaluated using the enzyme-linked immunosorbent assay (ELISA),[21] and the procedure followed that described previously.[22,23] Polyurethane films with 1.0 × 1.0 cm^2 surface area were incubated with 500 μL of Phosphate Buffered Saline (PBS) at 37 °C for 60 min, and were then incubated sequentially with 500 μL of 0.5 mg mL^{-1} human fibrinogen (Fg, F3879, 55–75% protein, purchased from Sigma, Shanghai) in PBS solution at 37 °C for 120 min, 500 μL of bovine serum albumin (BSA, 2 mg mL^{-1}) in PBS solution at 37 °C for 90 min, and 500 μL of 5.5 μg mL^{-1} horseradish peroxidase (HRP) conjugated goat anti-human fibrinogen (RCe-0363G, Y-Y Chemical Reagents, Shanghai) in PBS solution at 37 °C for 30 min. The polyurethane films were rinsed 5 times with 500 μL of washing buffer and transferred into clean wells, and the enzyme-induced color change reaction was then carried out by adding 500 μL of 0.1 M citrate-phosphate buffer (pH = 5.0) containing 1 mg mL^{-1} chromogen of *o*-phenylenediamine (OPD) and 0.03% hydrogen peroxide, and finally the absorbance of light at 490 nm was determined by a microplate reader (Model 550, Bio-Rad, USA). The absorbance from the control poly(ether urethane) films was equivalent to 100% for calculating relative adsorption values. Four replicate samples were measured for each concentration in a given experiment. Experiments were done three times.

2.3.8. Platelet adhesion assay. Platelet adhesion measurements were carried out according to the standard protocol as described briefly below. Fresh blood from healthy, drug-free donors was collected using vacuum tubes, containing sodium citrate as an anticoagulant (anticoagulant and blood with the volume ratio 1 : 9), and platelet-rich plasma (PRP) was obtained from blood centrifuged at 190*g* for 10 min. The polyurethane films (10 mm × 10 mm) were placed into a 24-well tissue culture plate and were immersed in 1.0 mL PBS (pH 7.4) and equilibrated at 37 °C for 1 h. After the PBS was removed, 1.0 mL PRP was poured into each well, and the films were soaked in the PRP

for 2 h at 37 °C. After the PRP solution was removed, the films were rinsed 3 times with PBS (3 × 1.0 mL), and then treated with 2.5% glutaraldehyde for 1 day at 4 °C. After rinsing with PBS solution, the films were dehydrated with a series of composition gradients of aqueous ethanol solutions (ethanol composition: 0%, 25%, 50%, 75% and 100%). Critical point drying of the specimens was done with liquid CO_2. The dried films were gold coated and then examined with a JEOL Superprobe 733 (JEOL, Japan) scanning electron microscope at 20 kV. Quantitative measurements were made for 5 representative areas of 12 different specimens by image analysis.

2.4. Statistical analysis

All data are expressed as the mean ± standard deviation. One-way ANOVA with Tukey *post hoc* tests were used for hypothesis testing, with $p < 0.05$ as the measure for statistical significance. The number of independent tests has been listed for each experiment.

3. Results and discussion

3.1. Synthesis of end-capping reagents and polyurethanes

To explore the influence of the fluorocarbon chain and phosphorylcholine on the improvement of blood compatibility in polyurethanes, three monomers with characteristic structures were designed and synthesized, and then were utilized to end-cap polyurethanes. The synthetic routes are shown in Schemes 1 and 2.

As shown in Scheme 1, each of the three end-capping reagents contains an amine ($-NH_2$) as the active functional group to block polyurethane chains, while each of them also has its own distinctive structure. Monomer I ("FA" for short) is based on perfluorooctanoic acid, and the main structure of FA was confirmed through MS and ^{1}H NMR results, which are listed in the Experimental section. The synthesis of monomer II (APPC) was based on 5-amino-1-pentanol, 2-choloro-1,3,2-dioxaphospholane-2-oxide (COP) and trimethylamine according to the Ishihara method.[24] The phosphorylcholine polar head (PC) is the

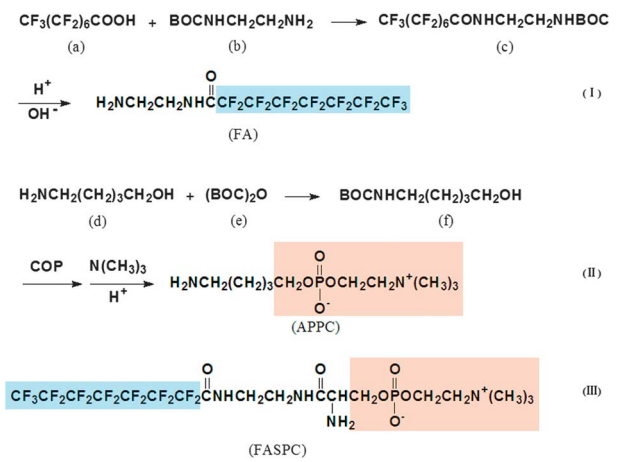

Scheme 1 The synthesis routes and structures of the monomers.

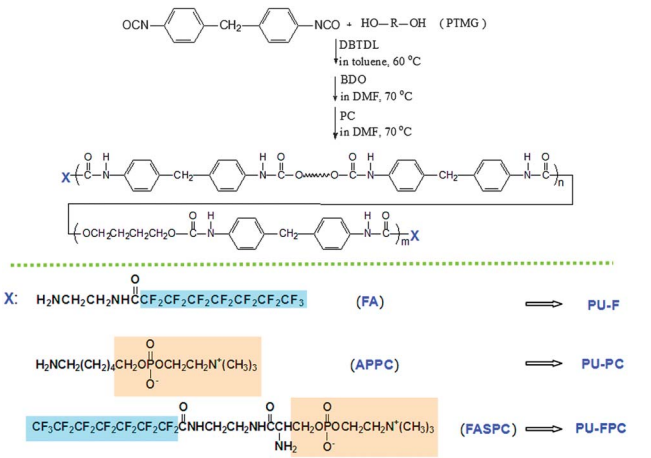

Scheme 2 The synthesis of polyurethanes end-capped with monomers.

biomimetic functional group. Monomer III (FASPC) was synthesized according to our previous study.[22,23] In this molecule, the PC head group and long fluorinated tail are both linked to L-serine, and the amine in L-serine is retained as an active group. These three monomers decorated with active amines could provide the reactivity with the isocyanato group of MDI, and thus endow the polyurethanes with distinctive features.

It is possible to achieve a broad range of properties by varying the hard and soft segments of polyurethanes.[25,26] In our previous work, FASPC was introduced into various polyurethanes, and the hemocompatibility of all samples were obviously improved without specificity.[23] MDI, PTMG and BDO were chosen to synthesize the control polyurethane, which are also the components of some commercial polyurethanes (*e.g.*, pellethane). The stoichiometries of the reaction are shown in Table 1, and the detailed descriptions of the syntheses are presented in the Experimental section. The control polyurethane and FA, APPC, FASPC end-capped polyurethanes were labeled as PU, PU-F, PU-PC and PU-FPC, respectively.

GPC, ^{1}H NMR, XPS, and element determination were used to confirm the structure and composition of the polyurethanes. The weight-average molecular weight (M_w) and number-average molecular weight (M_n) of the polyurethanes were determined by GPC (as shown in Table 1), and calibrated based on narrow molecular weight PMMA standards. It is shown that all their average molecular weights are on the order of 10^4 (between 2.69×10^4 and 5.67×10^4 in M_n). Due to the leaching of unreacted end-cappers and the low molecular weight fraction in methanol–distilled water mixed solvent and the nature of solution polymerization, the polydispersities of the polyurethanes are all less than 2.0.

The results of ^{1}H NMR are shown in the Experimental section. The characteristic peak of phosphorylcholine ($-N^+(CH_3)_3$) at 3.13 ppm appears clearly in both PU-PC and PU-FPC. The characteristic peak of FA does not appear obviously in PU-F due to the small fraction of characteristic hydrogen atoms ($-CF_2-CH_2-$). However, the successful end-capping can be verified by the results of XPS and F/P element determinations, the results of which are listed in Table 2. The appearance of F

Table 1 Stoichiometry, molecular weights and yields of the polyurethanes

Sample	Stoichiometry MDI : PTMG : BDO : end-capper	Molecular weight[a] $M_n \times 10^{-4}$	$M_w \times 10^{-4}$	M_w/M_n	Yield (%)
PU	3 : 2 : 1 : 0	5.67	8.53	1.50	78
PU-F	3 : 2 : 0.5 : 1	2.75	4.87	1.77	71
PU-PC	3 : 2 : 0.5 : 1	2.69	4.64	1.72	82
PU-FPC	3 : 2 : 0.5 : 1	3.50	5.68	1.62	75

[a] Gel permeation chromatography (GPC) was performed with a Waters-1515 using *N*,*N*-dimethylformamide (DMF)–LiBr as eluent. The molecular weights are relative to polymethyl methacrylate (PMMA) standards.

and/or P elements in PU-F, PU-PC, and PU-FPC is direct evidence for the successful end-capping synthesis. The F content in the bulk of PU-FPC is lower than that in PU-F, and the same trend is observed in the comparison of P content between PU-FPC and PU-PC. It is assumed that the FASPC monomer has lower reactivity than FA and APPC due to steric hindrance of the amine.

3.2. Structure analysis

As potential biomaterials, both the surface and bulk properties play important roles in the performance of polyurethane materials. Therefore, the surface chemical constitution and the phase separation of polyurethanes were examined after the introduction of end-cappers.

The XPS data could give direct and atomic scale chemical information about the surface groups. The atomic concentration of carbon (C 1s), oxygen (O 1s), nitrogen (N 1s), phosphorus (P 2p), and fluorine (F 1s) in the 5–10 nm depth range from the surface were detected.[23,27] The C 1s peaks in the four kinds of polyurethanes were fitted to seven component peaks. Among them, the CF_2 and CF_3 peaks belong to the fluorinated tail, which appear in the C 1s spectra of PU-F and PU-FPC. The C–O–P peak belonging to PC group appears in the C 1s spectra of both PU-PC and PU-FPC. However, the C–O–P peak area of PU-FPC is much larger than that of PU-PC, as shown in Fig. 1a and c. For composition, the weight contents of F and P in the bulk were also detected by the element determination method, and the results are also shown in Table 2. The atomic percentages of F and P on the surface were calculated as a weight percentage to adapt to the values in the bulk. The wt% of F on the surfaces of PU-F and PU-FPC are 48.71% and 37.72% (ignoring the hydrogen fraction), which are 6.3 times and 37.03 times to that in the bulk; the wt% of P in PU-PC and PU-FPC on the surface are 2.5 times and 5.8 times that in the bulk, respectively. The results indicate that the chain ends of polyurethane possess high mobility and tend to migrate to the surface. However, the end-capping of the PC group on polyurethane chains has limited effect on migration, compared to the easier migration of the FA and FASPC groups.

Microphase separation is the main concern for polyurethanes, which plays an important role in determining the surface and bulk properties.[28,29] In this work, dynamic mechanical analysis (DMA) was employed to study the thermal transitions of the polyurethanes, and the changes in glass transition temperature (T_g) of the soft segment phase determined from the peaks of tan δ curves were used as an indicator of the degree of phase separation.[29] The DMA data are shown in Fig. 2A, and the T_g data are listed in Table 3. The T_g values of the end-capped polyurethanes are all lower than that of the control sample, which suggests a trend of enhanced microphase separation in the bulk.

Fluorinated groups are considered as microphase segregating groups, where the perfluoro moiety prefers to be separated from the aliphatic groups and tends to assemble at the

Table 2 Element contents of polyurethanes on the surface and in the bulk

Sample	Element contents on the surface[a] (at%) C	O	N	P	F	Element contents in the bulk[b] (wt%) P	F
PU	76.27	21.90	1.83	0	0	—	—
PU-F	48.81	7.65	4.79	0	38.75	0	7.67 ± 0.26
PU-PC	77.48	19.73	2.50	0.29	0	0.28 ± 0.02	0
PU-FPC	51.94	12.07	6.16	0.53	29.30	0.19 ± 0.06	1.02 ± 0.01

[a] Values detected by XPS. [b] Values detected by element determination; "—" not detected.

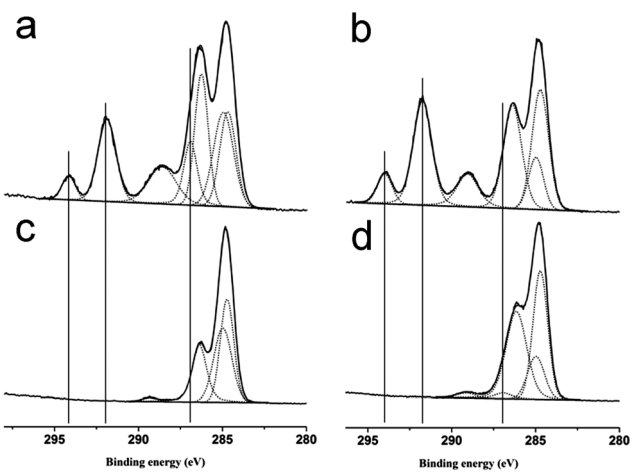

Fig. 1 C 1s XPS spectra of PU-FPC (a), PU-F (b), control PU (c), and PU-PC (d).

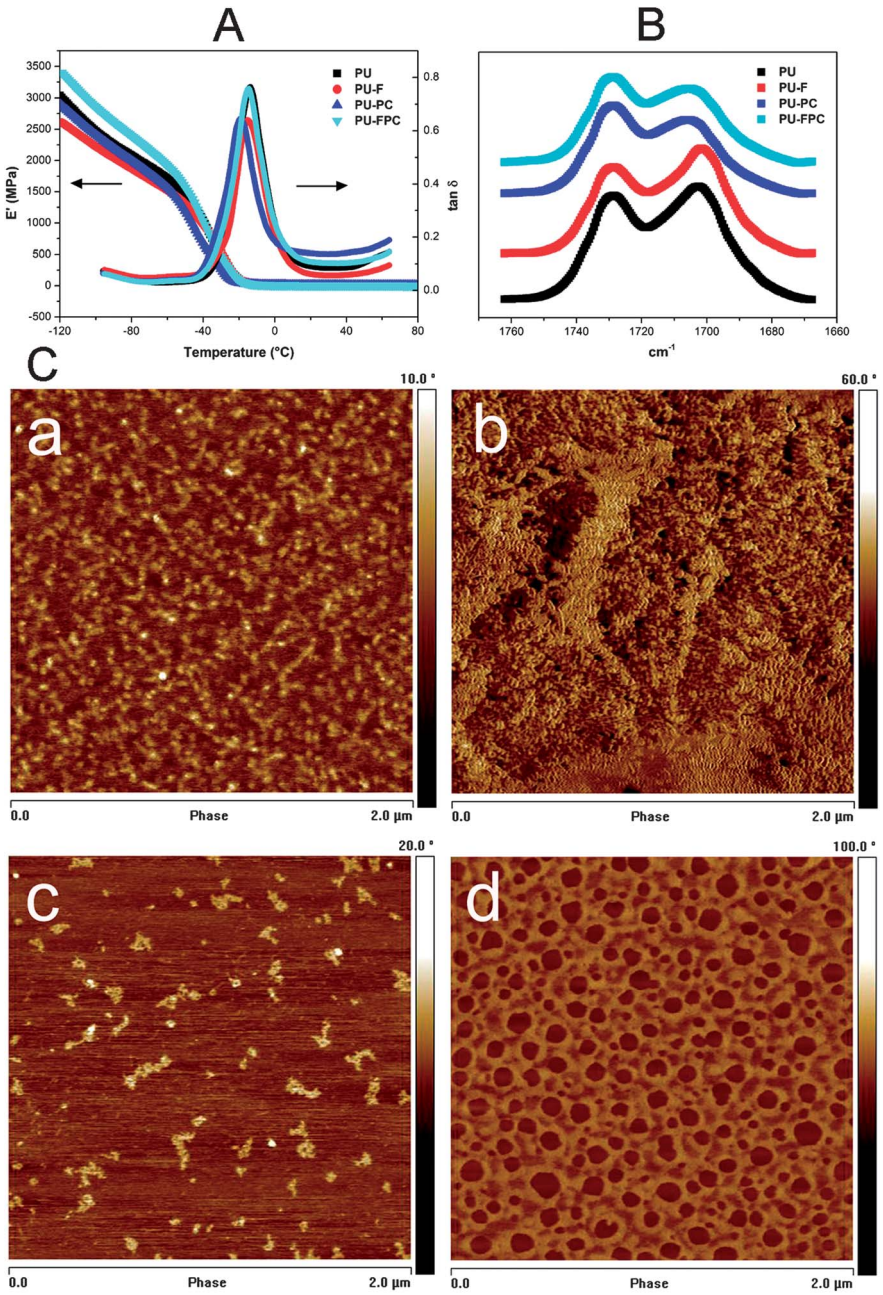

Fig. 2 (A) Dynamic mechanical spectra of polyurethanes; (B) C═O stretching band in the FTIR spectra of polyurethanes; (C) AFM phase images of control PU (a), PU-F (b), PU-PC (c), and PU-FPC (d).

Table 3 Glass transition temperatures detected by DMA, and C═O stretching band information of the polyurethanes

		"Free" C═O		H-bonded C═O	
Sample	T_g of soft segment (°C)	Stretching band ν (cm^{-1})	Area percentage (%)	Stretching band ν (cm^{-1})	Area percentage (%)
PU	−17.05	1729	37.8	1707	62.2
PU-F	−18.88	1729	39.7	1706	60.3
PU-PC	−24.31	1730	40.4	1704	59.6
PU-FPC	−18.33	1730	38.7	1702	61.3

interface,[30–32] therefore the enhanced microphase separation results in a lower T_g of the soft segment of PU-F than that of the control PU. Zwitterions in block polymers usually play the role of a "binder" between two phases and cause strong microphase separation.[33,34] Moreover, the steric hindrance of the phosphorylcholine group with the hard segment and soft segment further strengthens the microphase separation of PU-PC, and therefore the T_g of the soft segment of PU-PC is lowest of the four kinds of polyurethanes. As for PU-FPC, since the fluorocarbon chain and the PC group are linked, the weak intermolecular forces acting on the fluorocarbon chains can partly shield the polarizable environment offered by the PC group,[35] and this shield effect inhibits the improvement of microphase separation and results in a higher T_g compared with that of PU-PC.

In the infrared spectra of polyurethanes, the amide I band, which is principally due to carbonyl stretching vibration modes, has a relatively well-resolved adsorption doublet. The higher wavenumber peak (at about 1730 cm^{-1}) is associated with "free" (non-bonded) C═O stretching adsorption, and the lower wavenumber peak (at about 1710 cm^{-1}) mainly represents the adsorption of hydrogen-bonded C═O (with –NH– groups) in hard segments.[36,37] Therefore, the area and wavenumber of the H-bonded carbonyl peak can reflect the morphology of the hard segment in polyurethanes. The analysis of the FTIR spectra shown in Fig. 2B makes use of the above general assignments for the C═O stretching adsorption. To quantitate the examination of the carbonyl stretching band, the resolution results of the C═O peaks are listed in Table 3.[38] As observed in the FTIR data, upon careful examination of the C═O band, it is evident that the peak area of the H-bonded C═O stretching band decreases after end-capping, which indicates that the content of the hard segment decreases in the bulk of PU-F, PU-PC and PU-FPC. In addition, all the H-bonded C═O bands of end-capped polyurethanes show a similar trend of shifting to lower wavenumbers, which should be due to the improvement of microphase separation compared with conventional polyurethane.[39,40]

According to the analysis of infrared spectroscopy and DMA data, the enhanced microphase separation between soft segments and hard segments is due to the introduction of a fluorinated tail and/or phosphorylcholine group. In addition, the hard segment contents of all the end-capped polyurethanes are decreased in the bulk.

AFM was used to further investigate the microphase structure of the polyurethane surface in the form of visualization, as shown in Fig. 2C. Working at tapping mode, the phase image provides information about surface stiffness variation related to changes in Young's modulus, and the microphase-separated structures can be seen in the phase images.[29,41,42] The light color regions generally represent the hard segment due to its higher modulus.

It should be noted that the contrast in phase images is based on the same level of tapping force (amplitudes with range 0.4–0.7). A typical microphase separation pattern is displayed in the phase image of the control PU, and the hard segment phase size is uniformly dozens of nanometers. However, the introducing of end-capping groups changes the surface microdomains of the polyurethanes drastically. The fluorocarbon chains of PU-F, which are decorated on the hard segment, drive the hard segment to the surface due to the lower surface energy, and the hard domains almost cover the surface of PU-F.[41] This result is in agreement with the XPS data. In the phase image of PU-PC, a decrease in the content of hard domains is observed, while the size of them increases obviously and the boundary between hard domains and soft domains becomes sharper than that in the PU phase image. The phase inversion is complete in the PU-FPC phase image. Driven by the fluorinated tail, the hard domains aggregate on the surface and become a continuous phase, and the soft domains become the dispersion phase with "island" shape, as shown in Fig. 2C and D. The comparision of surface phase morphology between PU and the end-capped polyurethanes in the AFM data confirms the similar trend of enhanced microphase separation behavior for the end-capped polyurethanes as that observed in the DMA and FTIR analysis. The surface hard segment content of PU-PC is less than that of PU, while the surface hard segment contents of PU-F and PU-FPC are much greater than that of PU, which is the reverse of the trend detected in the FTIR spectra. It can be deduced that the surface morphologies of the end-capped polyurethanes, especially PU-F and PU-FPC, are different from the morphologies in the bulk, which corresponds to the chemical variation from bulk to surface detected by XPS, and the fluorocarbon chains play an important role in this system.

3.3. Surface properties

The time-related water contact angles on the surfaces of the polyurethane films were determined, and typical images are shown in Fig. 3a. It can be observed that the water drops on all the polyurethane films show relatively stable contact angles: the change from momentary angles to equilibrium values in 40 seconds is less than 10°. The high values of the water contact angles on PU-F and PU-FPC films (above 115°) are caused by the appearance of fluorocarbon chains on the surfaces, which has been verified by XPS data. The angles of PU-PC are slightly lower than that of PU due to the phosphorylcholine groups on the surface. The results indicate that the fluorocarbon chains tend to cover the top surface to minimize the surface free energy after the polyurethane films are formed, while the phosphorylcholine groups do not show this trend.

To investigate the rearrangement ability, the polyurethane films were soaked in distilled water at room temperature for one week, and then the water contact angles were determined again after drying under nitrogen, the results of which are shown in Fig. 3b. The water contact angle pictures of PU-FPC are also shown for comparison. After the water treatment, all the end-capped polyurethane films have lower water contact angles than the control PU film. This result could be explained by the restructuring of the surface structure:[43–45] after water penetration into the surface and consequent reconstruction of the atoms and molecules at the surface of the substrate, some of the strongly hydrophobic fluorocarbon chains migrate to the subsurface, and the hydrophilic structures, mainly phosphorylcholine groups in this system, tend to migrate to the top

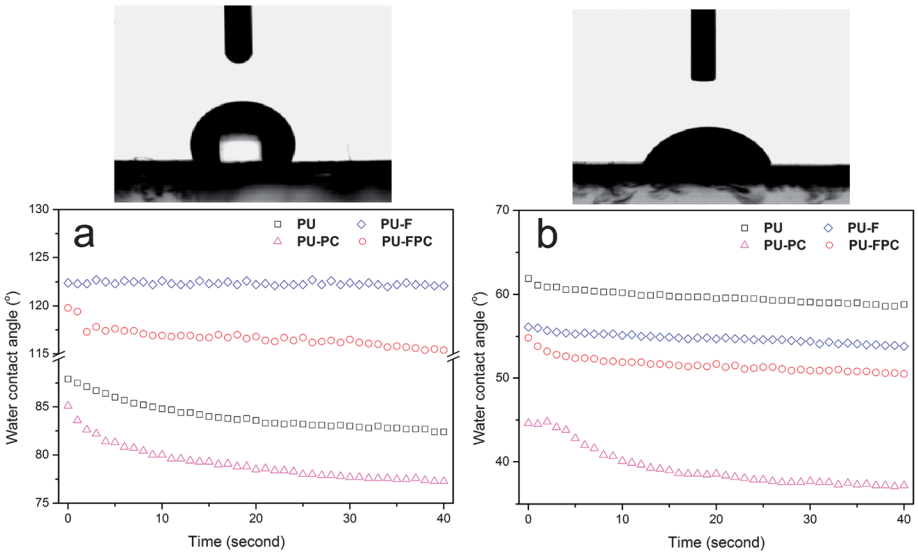

Fig. 3 The water contact angles of polyurethanes before (a) and after (b) water treatment for one week. The water contact angle pictures are of the PU-FPC sample.

surface. The strong mobility of fluorocarbon chains is demonstrated in this process. However, since the fluorocarbon chain are linked with the phosphorylcholine group on the molecular scale, it should have an effect on the improvement of the hydrophility of the whole FASPC moiety for PU-FPC, and it could be understood that the PU-FPC film with more phosphorylcholine groups on the surface has a higher water contact angle than the PU-PC film.

3.4. Hemocompatibility evaluation

Platelet adhesion and activation on the surface of blood-contacting devices will trigger the coagulation of blood leading to thrombus formation, and protein adsorption is the first step in a cascade of surface processes that induce platelet deposition and thrombus formation. Thus, protein adsorption and platelet adhesion are usually investigated as a preliminary evaluation of the hemocompatibility of materials,[46–48] which have also been employed in this work.

Fibrinogen (Fg) is one of the most abundant proteins in blood and plays a vital role in thrombosis on the surface of materials, and the adsorption of human fibrinogen on polyurethane films was detected by the ELISA method in this study. This testing method cannot obtain absolute values for the amount of Fg adsorbed on a film surface in units ($\mu g\ cm^{-2}$),[21,49] so the Fg adsorption to the control PU film was used as a reference, and the relative Fg adsorptions on the end-capped polyurethane films with respect to that on the PU film are shown in Fig. 4. In comparison with the control PU, the amount of adsorbed human Fg on PU-F, PU-PC, and PU-FPC decreased by 23.5%, 37.6%, and 78.7%, respectively. Even though the surface of PU-F is covered by fluorocarbon chains, the decrease of adsorbed Fg on PU-F is still less than that of PU-PC, which indicates that the phosphorylcholine groups are more effective than the fluorocarbon chain for the resistance to protein adsorption. The PU-FPC sample shows the lowest amount of Fg adsorption, which can be mainly attributed to the greater number of phosphorylcholine groups. In this preliminary evaluation, Fg adsorption was measured as a single reference to evaluate the protein adsorption. However, it is important to note that other plasma proteins (such as von Willebrand factor, plasminogen or fibronectin), which also play important roles in the coagulation process,[50,51] were not tested in this study.

Fig. 5 shows typical SEM photographs of platelet adhesion to the polyurethane films. In this study, the blood platelets from multiple donors (three donors) were taken for the test, with the aim of avoiding potential donor-to-donor variations in platelets and their reactivity/adhesion to surfaces.[50,52] Statistically analyzed by images of parallel samples, the platelet counts on the surfaces of PU, PU-F, and PU-PC are $(1.7 \pm 0.5) \times 10^6\ cm^{-2}$, $(4.1 \pm 1.4) \times 10^4\ cm^{-2}$, and $(2.9 \pm 0.6) \times 10^5\ cm^{-2}$, respectively. On the surface of PU-FPC, hardly any platelets can be found after soaking for 2 h. There are not only a substantial number of adhered platelets, but also some deformed platelets on the

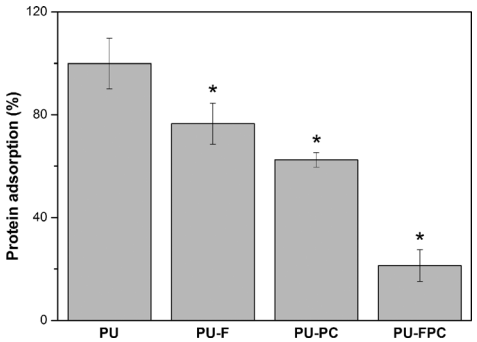

Fig. 4 Relative human fibrinogen adsorption on various polyurethanes determined from ELISA with control PU as a reference. * Statistically significant difference with respect to control PU ($p < 0.05$).

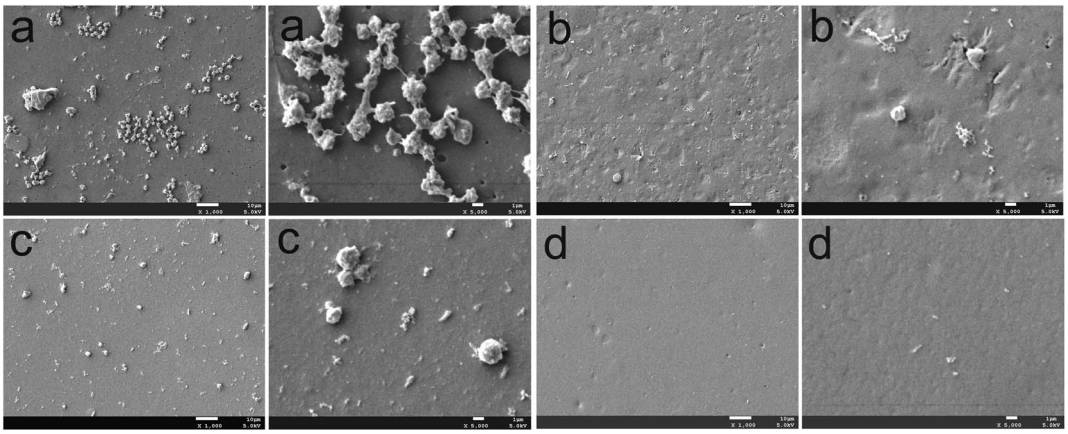

Fig. 5 SEM images of the surfaces of polyurethane films after 2 h of PRP exposure. (a) PU; (b) PU-F; (c) PU-PC; (d) PU-FPC. Actual magnification: left 1000× ; right 5000×.

surface of the control PU, which indicates that activation of the adhered platelets may occur. Most of the platelets adhered on the PU-F and PU-PC surfaces remained a normal shape.

The varying degrees of resistance to protein adsorption and platelet adhesion by phosphorylcholine groups and fluorocarbon chains in polyurethanes is an interesting phenomenon in this study. It has been reported that both fluorocarbon chains and PC groups on a polymer surface can prevent protein adsorption and platelet adhesion to improve blood compatibility.[12,20,53] The experimental data in this study also verify this trend, while the degree of improvement in each aspect is different. In the protein adsorption study, the number of PC groups present on the surface of PU-PC is much lower than that of fluorocarbon chains at the PU-F surface (from XPS and AFM data), but the amount of fibrinogens adsorbed on PU-PC is still lower than that on PU-F, which obviously indicates the greater efficiency of the PC group in preventing protein adsorption. The opposite trend is observed in the platelet adhesion experiment. The amount of platelets adhered to PU-F is one order of magnitude smaller than that adhered to PU-PC, which means that the fluorocarbon chains in PU-F reduce the adhesion of platelets more efficiently than PC groups in PU-PC. It can be concluded that, in polyurethanes, the fluorocarbon chains are more efficient for resisting platelet adhesion, while the PC groups prevent fibrinogen adsorption more effectively. Moreover, when fluorocarbon chains and PC groups are simultaneously introduced into polyurethane, the hemocompatibility (in both protein adsorption and platelet adhesion experiments) is improved dramatically in this preliminary study. This synergistic effect triggered by two anticoagulation components in polyurethane is promising, and is worthy of quantitative research in detail and in other materials in the future.

4. Conclusions

In this work, three monomers containing a fluorinated tail and/or phosphorylcholine for end-capping were synthesized and introduced into polyurethanes. It is found that the fluorocarbon chains and phosphorylcholine groups have a synergistic effect on the improvement of hemocompatibility of the polyurethanes, and the advanced properties are mainly due to these reasons:

(1) The migration ability of the fluorocarbon chains can drive the phosphorylcholine groups to the surface of the polyurethane films.

(2) The spontaneous arrangement of fluorocarbon chains and phosphorylcholine groups results in a balance on the surface to adapt to the water environment.

(3) Both fluorocarbon chains and phosphorylcholine groups in polyurethanes have their own advantages for anticoagulation, and each of them can play a vital role in preventing the progress of a clotting cascade.

Although the synergistic effect of fluorocarbon chains and phosphorylcholine groups on anticoagulation still needs to be further clarified in detail and *in vivo*, the results of this work indicate that the combination of anticoagulation components in the same material has real potential to develop biomaterials for contact with blood.

Acknowledgements

This work is a collaborative research project sponsored by the Ministry of Science and Technology of China (grant no. 2010DFA31190) and the Government of Quebec, Quebec, Canada (grant no. PSR-SIIRI-285). We would also like to express our sincere thanks to the National Natural Science Foundation of China for financial support (51121001).

Notes and references

1 H. S. Lee, N. Tomczyk, J. Kandel, R. J. Composto and D. M. Eckmann, *J. Mater. Chem. B*, 2013, **1**, 6382–6391.
2 F. Tong, X. Chen, L. Chen, P. Zhu, J. Luan, C. Mao, J. Bao and J. Shen, *J. Mater. Chem. B*, 2013, **1**, 447–453.
3 R. Y. Kannan, H. J. Salacinski, P. E. Butler, G. Hamilton and A. M. Seifalian, *J. Biomed. Mater. Res., Part B*, 2005, **74B**, 570–581.

4 K. Kashimoto, J. Yoon, B. Y. Hou, C. H. Chen, B. H. Lin, M. Aratono, T. Takiue and M. L. Schlossman, *Phys. Rev. Lett.*, 2008, **101**, 076102.
5 I. Lee, K. Kobayashi, H. Y. Sun, S. Takatani and L. G. Zhong, *J. Biomed. Mater. Res., Part A*, 2007, **82A**, 316–322.
6 H. Yin, T. Akasaki, T. L. Sun, T. Nakajima, T. Kurokawa, T. Nonoyama, T. Taira, Y. Saruwatari and J. P. Gong, *J. Mater. Chem. B*, 2013, **1**, 3685–3693.
7 A. P. Khandwekar, D. P. Patil, A. A. Hardikar, Y. S. Shouche and M. Doble, *J. Biomed. Mater. Res., Part A*, 2010, **95A**, 413–423.
8 R. Leitsmann, O. Bohm, P. Planitz, C. Radehaus, M. Schaller and M. Schreiber, *Surf. Sci.*, 2010, **604**, 1808–1812.
9 X. Y. Xie, R. F. Wang, J. H. Li, L. Luo, D. Wen, Y. P. Zhong and C. S. Zhao, *J. Biomed. Mater. Res., Part B*, 2009, **89B**, 223–241.
10 T. Hong, X. Xingyi, L. Jiehua, Z. Yingping and F. Qiang, *Polymer*, 2004, **45**, 1495–1502.
11 G. Jiang, X. Tuo, D. Wang and Q. Li, *J. Mater. Sci.: Mater. Med.*, 2012, **23**, 1867–1877.
12 K. Y. Chen and J. F. Kuo, *J. Mater. Sci.: Mater. Med.*, 2002, **13**, 37–45.
13 J. C. Lin, S. L. Tiong and C. Y. Chen, *J. Biomater. Sci., Polym. Ed.*, 2000, **11**, 701–714.
14 H. Wang, F. Xu, Y. Wang, X. Liu, Q. Jin and J. Ji, *Polym. Chem.*, 2013, **4**, 3012–3019.
15 P. Wan, D. Tan, Z. Li, X. Zhang, J. Li and H. Tan, *Chin. J. Polym. Sci.*, 2012, **30**, 190–198.
16 T. Goda, H. Furukawa, J. P. Gong and K. Ishihara, *Soft Matter*, 2013, **9**, 2166–2171.
17 M. Tan, Y. Feng, H. Wang, L. Zhang, M. Khan, J. Guo, Q. Chen and J. Liu, *Macromol. Res.*, 2013, **21**, 541–549.
18 T. Hatakeyama, M. Tanaka and H. Hatakeyama, *Acta Biomater.*, 2010, **6**, 2077–2082.
19 K. Ishihara, H. Nomura, T. Mihara, K. Kurita, Y. Iwasaki and N. Nakabayashi, *J. Biomed. Mater. Res.*, 1998, **39**, 323–330.
20 Y. Iwasaki, Y. Aiba, N. Morimoto, N. Nakabayashi and K. Ishihara, *J. Biomed. Mater. Res.*, 2000, **52**, 701–708.
21 Z. Zhang, T. Chao, S. F. Chen and S. Y. Jiang, *Langmuir*, 2006, **22**, 10072–10077.
22 D. Tan, X. Zhang, J. Li, H. Tan and Q. Fu, *J. Biomed. Mater. Res., Part A*, 2012, **100A**, 380–387.
23 X. Zhang, D. Tan, J. Li, H. Tan and Q. Fu, *Biofouling*, 2011, **27**, 1175.
24 K. Ishihara, T. Uchida and N. Nakabayashi, *Polym. J.*, 1990, **22**, 355–360.
25 Y. W. Tang, R. S. Labow and J. P. Santerre, *J. Biomed. Mater. Res.*, 2001, **56**, 516–528.
26 T. Choi, J. Weksler, A. Padsalgikar and J. Runt, *Polymer*, 2009, **50**, 2320–2327.
27 J. Tan and J. L. Brash, *J. Appl. Polym. Sci.*, 2008, **108**, 1617–1628.
28 L. C. Xu, J. Runt and C. A. Siedlecki, *Acta Biomater.*, 2010, **6**, 1938–1947.
29 H. Tan, J. H. Li, M. Guo, R. N. Du, X. Y. Xie, Y. P. Zhong and Q. Fu, *Polymer*, 2005, **46**, 7230–7239.
30 S. J. Cowling, A. W. Hall and J. W. Goodby, *J. Mater. Chem.*, 2011, **21**, 9031–9042.
31 G. De Luca, A. Liscio, M. Melucci, T. Schnitzler, W. Pisula, C. G. Clark, Jr, L. M. Scolaro, V. Palermo, K. Muellen and P. Samori, *J. Mater. Chem.*, 2010, **20**, 71–82.
32 Y. Zhang, L. Wang, Z. Zhang, Y. Zhang and X. Tuo, *J. Polym. Sci., Polym. Chem. Ed.*, 2013, **51**, 2161–2170.
33 E. Marwanta, T. Mizumo and H. Ohno, *Solid State Ionics*, 2007, **178**, 227–232.
34 S. Pispas, G. Floudas and N. Hadjichristidis, *Macromolecules*, 1999, **32**, 9074–9077.
35 X. Wang, P. Long, S. Dong and J. Hao, *Langmuir*, 2013, **29**, 14380–14385.
36 M. M. Coleman, D. J. Skrovanek, J. Hu and P. C. Painter, *Macromolecules*, 1988, **21**, 59–68.
37 D. Tan, X. Zhang, J. Li, H. Tan and Q. Fu, *Appl. Surf. Sci.*, 2012, **258**, 2697–2706.
38 D. Tan, X. Zhang, J. Li, H. Tan and Q. Fu, *Chin. J. Polym. Sci.*, 2011, **29**, 615–626.
39 D. A. Wang, J. Ji and L. X. Feng, *Macromolecules*, 2000, **33**, 8472–8478.
40 G. Trovati, E. Ap Sanches, S. C. Neto, Y. P. Mascarenhas and G. O. Chierice, *J. Appl. Polym. Sci.*, 2010, **115**, 263–268.
41 M. Penoff, W. Schreiner, P. Oyanguren and P. Montemartini, *Macromol. Symp.*, 2012, **321–322**, 186–190.
42 Y. Yanagihara, N. Osaka, S. Murayama and H. Saito, *Polymer*, 2013, **54**, 2183–2189.
43 X. Cui, S. Zhong, Y. Gao and H. Wang, *Colloids Surf., A*, 2008, **324**, 14–21.
44 S. Perutz, J. Wang, E. J. Kramer, C. K. Ober and K. Ellis, *Macromolecules*, 1998, **31**, 4272–4276.
45 D. L. Schmidt, R. F. Brady, K. Lam, D. C. Schmidt and M. K. Chaudhury, *Langmuir*, 2004, **20**, 2830–2836.
46 H. W. Chien, C. C. Tsai, W. B. Tsai, M. J. Wang, W. H. Kuo, T. C. Wei and S. T. Huang, *Colloids Surf., B*, 2013, **107**, 152–159.
47 J. Tan, W. G. McClung and J. L. Brash, *J. Biomater. Sci., Polym. Ed.*, 2013, **24**, 497–506.
48 L. Ma, H. Qin, C. Cheng, Y. Xia, C. He, C. Nie, L. Wang and C. Zhao, *J. Mater. Chem. B*, 2014, **2**, 363.
49 J. Li, Y. Zhang, J. Yang, H. Tan, J. Li and Q. Fu, *J. Biomed. Mater. Res., Part A*, 2013, **101A**, 1362–1372.
50 M. Zhang and T. A. Horbett, *J. Biomed. Mater. Res., Part A*, 2009, **89A**, 791–803.
51 L. M. Szott and T. A. Horbett, *Curr. Opin. Chem. Biol.*, 2011, **15**, 677–682.
52 J. M. Grunkemeier, W. B. Tsai and T. A. Horbett, *J. Biomed. Mater. Res.*, 1998, **41**, 657–670.
53 M. Pagliaro and R. Ciriminna, *J. Mater. Chem.*, 2005, **15**, 4981–4991.